FAST DYNAMIC MRI USING LINEAR DYNAMICAL SYSTEM MODEL

Vimal Singh,   Ahmed H. Tewfik

Electrical and Computer Engineering Department
The University of Texas at Austin, USA

ABSTRACT

Imaging of physiological functions using magnetic resonance imaging is limited due its slow data acquisition speed. Previously various techniques based on data sharing in the spatio-temporal k-space or sparse recovery methods have been proposed to increase imaging speeds in dynamic MRI. This paper presents a novel formulation for fast dynamic MRI which combines the generic linear dynamical system based spatio-temporal model with sparse recovery techniques. Specifically, the formulation uses a known prior time-evolution model for the physiological function implicitly and enforces the model errors (innovations) to be sparse. The preliminary results of dynamic MRI recovery experiments on an in-vivo myocardial perfusion dataset show that the proposed approach preserves details like edges and fine structures in recovered images better than previous k-space data-sharing and sparse recovery techniques individually.

Index Terms— MRI, Linear Dynamical System, Compressed Sensing, Sparse Innovations

1. INTRODUCTION

Magnetic resonance imaging is a slow imaging modality and many research studies over the past two decades have focused on improving its imaging speed. Many of the these studies are motivated by the emerging medical diagnostic procedures which rely on detailed characterization of physiological functions of critical organs such as cardiac and brain [1, 2]. The early studies (late 90s and early 2000s) were based on exploiting the redundancy in the raw data space (spatial Fourier a.k.a k-space) in either the spatial dimension or the temporal dimension or both [3, 4, 5, 6, 7]. More recent studies (after 2006) are based on the theory of compressed sensing (CS) which relies on recovering a transform of the underlying image in a basis where its representation is sparse and which exhibits high incoherency with the k-space sampling basis [8, 9, 10, 11, 12]. CS-based techniques for dynamic MR applications enforce sparsity in the spatial dimension or/and in the temporal dimension. Clearly, the techniques based on using sparsity priors in a single dimension are sub-optimal as the inherent redundancy in the complimentary dimension is unaccounted for. For other techniques, the sparsity priors in both dimensions are weakly coupled by the Lagrange constants used in the selected non-linear optimization problem. On the other hand, all physiological processes can be modeled using linear or non-linear evolution models. In these models the spatial and temporal redundancy is inherently coupled. Therefore, a sparse recovery formulation based on these evolution models for physiological functions should lead to recovered images with higher fidelity than previous techniques relying on single or weakly-coupled sparsity priors. In this paper, a linear dynamical system based evolution model is combined with sparse recovery techniques to increase the speeds in dynamic MRI applications.

Few studies in recent past have focused on combining the linear dynamical state estimation model with the sparse approximation methods. In [13], authors assume the states of the dynamical system to be sparse and separate the state estimation problem into two sub-problems of support and value estimation. Authors in [13] propose a CS-based ad-hoc Kalman filtering solution, where CS is used to estimate the support and the Kalman filter is run on the estimated support to track the states. Similarly, in [14] authors assume sparse states along with a zero-mean additive white Gaussian distribution for the state modeling noise. Their solution is based on adding a group-sparsity constraint to the established Kalman smoothing formulation. The added constraint (group-LASSO) forces groups of coefficients along the temporal dimension to zero. The aforementioned techniques assume the following: 1) the states are sparse and, 2) the state transition matrix for changing support of state vectors are always known. These two requirements are not necessarily true for dynamic MR applications where the underlying images represent the unknown states.

This paper presents a novel formulation for fast dynamic MR applications based on linear dynamical system (LDS) model. LDS models have been used previously to model various physiological processes such as: 1) blood flow in MR angiography and perfusion studies and, 2) periodic motion in cardiac and abdominal imaging [15, 16]. Thus, LDS models are generic and exhibit a wide applicability for modeling various dynamic MR applications. In the proposed formulation, similar to [13, 14], the underlying dynamic images are modeled as hidden states and the under-sampled k-space as the observed variables. However, unlike previous techniques the system innovations are assumed to be sparse instead of the states themselves, i.e., it is the error in state evolution model which is assumed to be sparse. The proposed formulation makes no assumptions about the underlying images like previous techniques [13, 14], however it requires knowledge of a time-evolution model for the underlying function. In future work, learning/adapting of this time evolution will also be investigated upon. This time-evolution model inherently encodes for data redundancies in both spatial- and temporal-space as opposed to techniques which explicitly account for these redundancies [7]. For example, the highly constrained back projection (HYPR) method of [7] enforces spatio-temporal redundancy by explicitly sharing high-frequency details between neighboring time-frames and oversampling the low-frequency information for each frame to capture the contrast information. The HYPR technique recovers sparse MR angiographic images at high acceleration factors ~ 25, however for not-so-sparse images gains of 4 only, have been reported. The preliminary results of dynamic MRI recovery experiments on an in-vivo myocardial perfusion dataset show that the proposed approach preserves details like edges and fine structures in recovered images better than a spatial-sparsity based CS-technique [9] and the HYPR technique [7] at all accelerations.

The rest of this paper is organized as follows. Section 2 presents a mathematical treatment of the linear dynamical system based fast dynamic MRI method. Section 3 summarizes the experimental results on an in-vivo myocardial perfusion data set. Finally, section 4 concludes the paper.

2. PROPOSED MODEL

This section presents a mathematical formulation for the proposed linear dynamical system based dynamic MRI model. Let x_k represent the Nx1 MR image acquired at k^{th} time-point for a physiological function. The dynamic MR imaging process in terms of the linear dynamical system is

$$x_{k+1} = \mathbf{A}_k \; x_k + u_k \tag{1a}$$
$$y_k = \mathbf{H}_k \; x_k + v_k \tag{1b}$$

where, $\mathbf{A}_k$ is the NxN state transition matrix, u_k is the innovation, y_k is the acquired k-space data, $\mathbf{H}_k$ is the MxN under-sampling matrix ($M \ll N$) and v_k is the sampling noise. In this work, following assumptions are made: 1) the state transition matrices $\mathbf{A}_k$'s are known and, 2) the noise u_k is sparse. These assumptions are true for various physiological functions. For example, in MR angiography and perfusion, within the imaged Field-of-View (FOV) the anatomical boundaries do not change over time but only the image-contrast varies over time. Thus, for angiography, $\mathbf{A}_k$ is the identity transform and the sparse innovations u_k models the contrast changes between time-points if any. For cardiac CINE studies, the state transition equation (1a) can be replaced with a 2^{nd} order auto-regressive model while still modeling the system innovations u_k as sparse. Sampling noise v_k is in the complex space and is assumed to be $\mathcal{N}(0, \mathbf{R}_k)$, where $\mathbf{R}_k$ is the covariance matrix.

An extensively studied case of the system (1) is the Kalman filter which assumes Gaussian statistics on both the sampling noise v_k and the system innovations $u_k \sim \mathcal{N}(0, \mathbf{Q}_k)$. The corresponding fixed-interval Kalman updater solves for the following problem

$$\min_{x_1,\ldots,x_k} \sum_{i=1}^{k} \tau_i \parallel x_i - \mathbf{A}_{i-1}x_{i-1}\|_2^2 + \sum_{i=1}^{k} \lambda_i \parallel \mathbf{H}_i x_i - y_i \parallel_2^2 \tag{2}$$

where, $\{\tau_i\}_{i=1}^k$ and $\{\lambda_i\}_{i=1}^k$ are the weight factors for the system innovations and sampling-noise models. Similarly, the fixed-interval solution for problem (1) with sparse u_k is

$$\min_{x_1,\ldots,x_k} \sum_{i=1}^{k} \tau_i \parallel x_i - \mathbf{A}_{i-1}x_{i-1}\|_1 + \sum_{i=1}^{k} \lambda_i \parallel \mathbf{H}_i x_i - y_i \parallel_2^2 \tag{3}$$

To solve (3), we can solve for $\{\widehat{u}_i\}_{i=1}^k$ and then use them to estimate $\{\widehat{x}_i\}_{i=1}^k$ explicitly using (1a). Similar solution was previously proposed in [17]. Now, the sparse innovations $\{\widehat{u}_i\}_{i=1}^k$ can be vectorized and rearranged as

$$\begin{bmatrix} u_1 \\ u_2 \\ \vdots \\ u_{k-1} \end{bmatrix} = \begin{bmatrix} \mathbf{I} & \mathbf{0} & \ldots & \mathbf{0} \\ -\mathbf{A}_1 & \mathbf{I} & \ldots & \mathbf{0} \\ \vdots & \vdots & \ddots & \vdots \\ \mathbf{0} & \ldots & -\mathbf{A}_k & \mathbf{I} \end{bmatrix} \begin{bmatrix} x_1 \\ x_2 \\ \vdots \\ x_{k-1} \end{bmatrix} - \begin{bmatrix} \mathbf{A}_0\widehat{x}_0 \\ 0 \\ \vdots \\ 0 \end{bmatrix}$$
$$\mathbf{u} = \mathcal{A}\mathbf{x} - \mathbf{z} \tag{4a}$$

where, $\widehat{x}_0$ is the initial estimate. Now, using (4) we can rearrange the second term in (3) as

$$\sum_{i=1}^{k} \parallel \mathbf{H}_i x_i - y_i \parallel_2^2 = \parallel \mathcal{H}\mathbf{x} - \mathbf{y} \parallel_2^2 \tag{5a}$$
$$= \parallel \mathcal{H}\mathcal{A}^{-1}\mathbf{u} - \left(\mathbf{y} - \mathcal{H}\mathcal{A}^{-1}\mathbf{z}\right) \parallel_2^2$$
$$= \parallel \mathcal{H}\mathcal{A}^{-1}\mathbf{u} - \widetilde{\mathbf{y}} \parallel_2^2 \tag{5b}$$

where, $\mathbf{y}$ is the vector obtained by stacking $\{y_i\}_{i=1}^k$ sampled vectors, $\widetilde{\mathbf{y}} = \mathbf{y} - \mathcal{H}\mathcal{A}^{-1}\mathbf{u}$ and $\mathcal{H}$ is obtained by stacking the sampling matrices $\{\mathbf{H}_i\}_{i=1}^k$ along the diagonal of kNxkM matrix. Note, in (5b), $\mathcal{A}^{-1}$ is simple to calculate due to the lower-triangle property of matrix $\mathcal{A}$. Using (1a) and (5b) in equation (3), the new fixed-interval optimal smoother is:

$$\min_{u_1,\ldots,u_k} \sum_{i=1}^{k} \parallel \mathbf{u} \parallel_1 + \frac{1}{2} \parallel \mathcal{H}\mathcal{A}^{-1}\mathbf{u} - \widetilde{\mathbf{y}} \parallel_2^2 \tag{6}$$

where, $\tau_i = 1, \lambda_i = 1 \forall i$ is assumed to yield the recognizable basis-pursuit denoising problem [18]. In (6), the dimensionality of the problem increases with k. For tractable problems, a sliding window based approach can be used. The solution to (6) for all experimental results presented in this paper are obtained using the the NESTA toolbox which implements the Nesterov's algorithm [19].

3. EXPERIMENTS AND RESULTS

The proposed linear dynamical system (LDS) based fast dynamic MRI technique is validated through retrospective under-sampling experiments on in-vivo myocardial perfusion data set (complex raw images). Following metrics are used to quantify the fidelity of recovered images in retrospective experiments : (1) SNR : signal-to-noise ratio and, (2) SSIM: structural similarity index [20]. In this paper, experimental results are presented for both 2DFT and radial under-sampled acquisitions. For radial under-sampling inverse-gridding is used to generate k-space data from complex raw images. In addition, the proposed technique is compared with 1) the standard Wavelet sparsity based CS technique [9] for 2DFT under-sampling and,

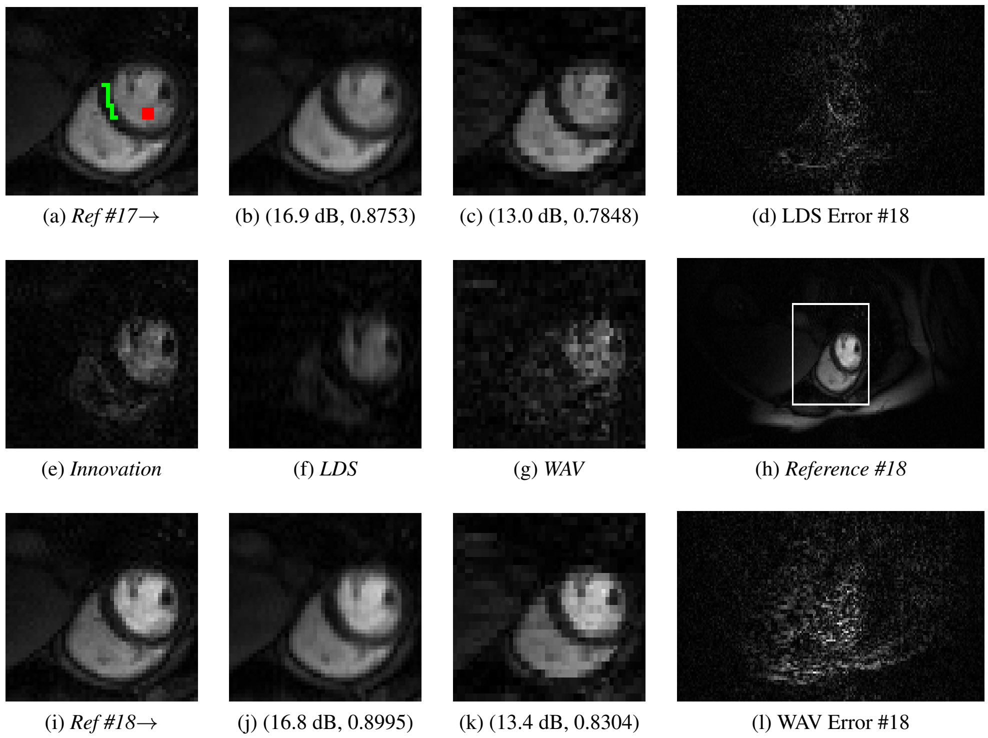

(a) *Ref #17*→ (b) (16.9 dB, 0.8753) (c) (13.0 dB, 0.7848) (d) LDS Error #18

(e) *Innovation* (f) *LDS* (g) *WAV* (h) *Reference #18*

(i) *Ref #18*→ (j) (16.8 dB, 0.8995) (k) (13.4 dB, 0.8304) (l) WAV Error #18

Fig. 1: Comparison of image recovery using the LDS and the WAV technique at an acceleration $R = 4$. (a) zoomed-in region from the reference image (f) of time-point (tp)#17. (i) zoomed region from reference tp#18. (e) shows the difference between (a) and (i), i.e., the *innovation* in the LDS technique. The second and third column show the recovered images and innovations for proposed LDS and the WAV technique, respectively. Performance for each technique is reported as pairs (SNR, SSIM) below the corresponding recovered images. (d) and (l) show the error images for the LDS (tp#17) and WAV (tp#18) technique, respectively.

2) the highly-constrained back-projection technique of [7] for radial under-sampling. For reasons of convenience the experimental results for the proposed technique will be referred to as LDS, for the Wavelet sparsity based CS technique as WAV and, for the technique of [7] as HYPR.

The perfusion data was acquired on a 3T Siemens scanner with a saturation-recovery sequence (TR\TE$= 2.5/1$ms, saturation recovery time$= 100$ms) and comprises of an image matrix of size 90x190x70 (phase-encodes x frequency encodes x temporal slices) [11]. Figure 1 shows the results for an retrospective variable density 2DFT under-sampling experiment at an acceleration factor of $R = 4$. For the LDS method, a sliding window of 4-samples (k in (4a)) is used and the initial state estimate $\widehat{x}_0$ is obtained by combining data from all time-points in the first sliding window and a taking a Fourier transform of it. Recovered images for two consecutive time-points (17 and 18) and the true and recovered innovation signal (u_{17} in (1a)) are shown for both the LDS and WAV techniques. The LDS technique estimates the innovation signal in fig. 1f using composite under-sampled data from 4-time-points and adds this innovation to fig. 1b to obtain the estimate for fig. 1j. The WAV technique treats each time-point independently and the innovation shown in 1g is calculated post-image-recovery. The LDS technique outperforms the WAV technique qualitatively and quantitatively as it inherently accounts for the temporal correlations which are not exploited in the WAV technique. The LDS technique shows much reduced under-sampling artifacts than the WAV technique, this can be observed in the error images of figs. 1d and 1l. Again, this can be attributed to inherent sharing of k-space information through the used time-evolution model which is absent in the WAV technique.

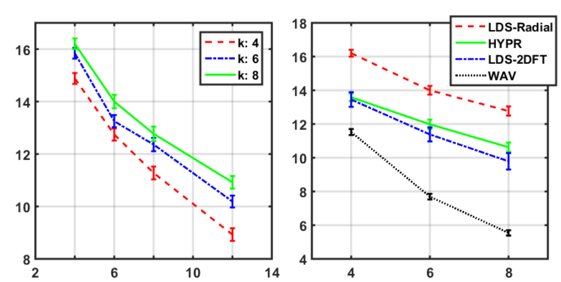

(a) *LDS* varying (k) (b) SNR vs. R

Fig. 3: ($\mu \pm \sigma$) SNR vs. R curves for: (a) varying sliding window size for *LDS technqiue*. (b) different techniques.

Results for the radial under-sampling experiments at an ac-

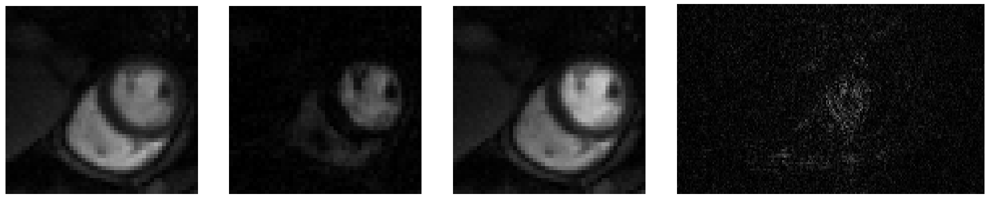

(a) (18.1 dB, 0.8839) (b) *LDS Innovation* (c) (18.1 dB, 0.9042) (d) LDS Error #18

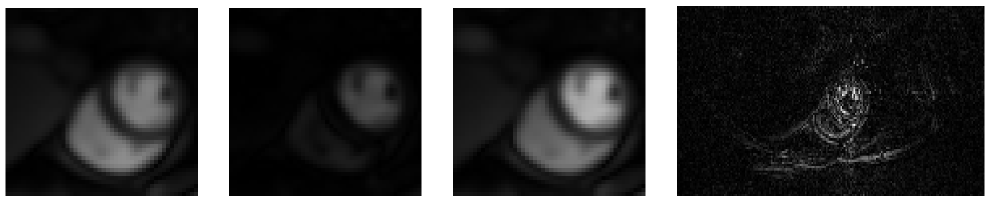

(e) (13.7 dB, 0.8279) (f) *HYPR Innovation* (g) (14.5 dB, 0.8637) (h) HYPR Error #18

Fig. 2: Comparison of image recovery using the LDS and HYPR techniques at an acceleration $R = 4$. (a) and (e) zoomed-in region from recovered images for time-point (tp) #17 for the LDS and HYPR technique, respectively. Similarly, (c) and (g) zoomed-in region from recovered images for tp#18. Corresponding innovations are shown in (b) and (f).(d) and (h) show the error images for the tp#18 for the LDS and HYPR technique, respectively. Performance for each technique is reported as pairs (SNR, SSIM).

celeration factor of $R = 4$ for the LDS and the HYPR [7] techniques are shown in figure 2. Due to limited space, only the recovered images, innovation and error images are shown. However, results are presented for the same time-points (# 17 and 18) as shown in fig. 1. Similar to the 2DFT experiments, the LDS method uses a sliding window of 4-samples and uses the image recovered using the HYPR technique as the initial state estimate $\widehat{x}_0$. In fig. 2, for both techniques no visible radial streaking artifacts are observed as they both use raw-data from multiple time-points to estimate each image. The HYPR technique results in smoothing of details and edges as seen in figs. 2e, 2f and 2g. This loss at edges is results in large errors at edges in fig. 2h. On the contrary, the proposed LDS technique uses combined data to estimate the innovation signal with sparsity constraint which does not adversely effects the image details. The LDS error image in fig. 2d shows discrepancies which are not localized to edges. For the LDS method the sliding window size can be varied (k in (4a)). Increasing k increases the dimensionality of the problem (6) and the sampled-data being used for estimating the sparse innovations. Figure 3a shows the (mean $\pm$ std. deviation) SNR versus acceleration (R) curves for varying k for the radial under-sampling experiment for the complete data set. Additionally, for deriving statistically relevant conclusion on relative performance of LDS (2DFT & radial), HYPR and WAV techniques, fig. 3b shows the corresponding SNR vs. R curves.

First-pass myocardial perfusion MRI is used to detect and evaluate ischemic heart disease [21]. Regional perfusion defects can be detected by analyzing the signal variability in an image time-series. Thus, to assess the applicability of a fast technique for myocardial perfusion imaging, time series plots of averaged signal intensity in selected blood pool and myocardium regions are critically evaluated. Figures 4a and 4b compare the time-series plots of averaged signal intensity in selected blood pool and myocardium regions in reference images with that of the recovered images at acceleration $R = 6$ using the *LDS* and the *HYPR* techniques, respectively. The selected blood pool (in red) and myocardium (in green) regions are shown in Figs. 1a. As expected, the time series curve for recovered images using the *LDS* technique follows the reference curve more closely than the curve for the *HYPR* technique.

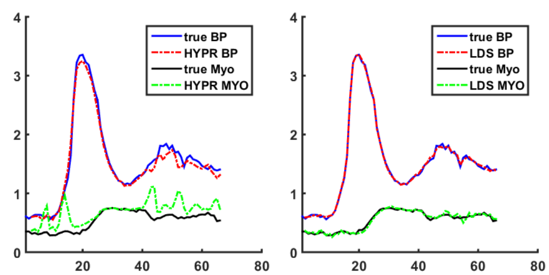

(a) *HYPR* (b) *LDS*

Fig. 4: Time-series plot of avg. signal for recovered (at R = 6) and reference images for the myocardial perfusion dataset.

4. CONCLUSIONS

This paper presents a novel dynamic MRI technique which assumes a prior time-evolution model for the underlying physiological function and enforces the model errors to be sparse. Further, the dynamic imaging problem is rearranged as the tractable basis pursuit de-noising problem. Preliminary results for dynamic MRI recovery experiments on an in-vivo cardiac data set are better than the previously established fast dynamic MRI methods based on variable density k-space sampling.

5. REFERENCES

[1] Hui Wang and A.A. Amini, "Cardiac Motion and Deformation Recovery From MRI: A Review," *IEEE Transactions on Medical Imaging*, vol. 31, no. 2, pp. 487 –503, Feb. 2012.

[2] Ze Wang, Sandhitsu R. Das, Sharon X. Xie, Steven E. Arnold, John A. Detre, and David A. Wolk, "Arterial spin labeled {MRI} in prodromal Alzheimer's disease: A multi-site study ," *NeuroImage: Clinical*, vol. 2, pp. 630–636, 2013.

[3] Xiaoping Hu and Todd Parrish, "Reduction of field of view for dynamic imaging," *Magnetic Resonance in Medicine*, vol. 31, no. 6, pp. 691–694, 1994.

[4] C.M. Tsai and D.G. Nishimura, "Reduced aliasing artifacts using variable-density k-space sampling trajectories," *Magnetic Resonance in Medicine*, vol. 43, pp. 452–458, 2000.

[5] D.C. Peters, F.R. Korosec, G.M. Thomas, W.F. Block, J.E. Holden, K.K. Vigen, and C.A. Mistretta, "Undersampled projection reconstruction applied to MR angiography," *Magnetic Resonance in Medicine*, vol. 43, pp. 91–101, 2000.

[6] J. Tsao, P. Boesiger, and K.P. Pruessmann, "k-t BLAST and k-t SENSE: Dynamic MRI with high frame rate exploiting spatio-temporal correlations," *Magnetic Resonance in Medicine*, vol. 50, no. 5, pp. 1031–1042, 2003.

[7] C. A. Mistretta, O. Wieben, J. Velikina, W. Block, J. Perry, Y. Wu, K. Johnson, and Y. Wu, "Highly constrained backprojection for time-resolved MRI," *Magnetic Resonance in Medicine*, vol. 55, no. 1, pp. 30–40, 2006.

[8] E.J. Candes, J. Romberg, and T. Tao, "Robust uncertainty principles: exact signal reconstruction from highly incomplete frequency information," *Information Theory, IEEE Transactions on*, vol. 52, no. 2, pp. 489 – 509, Feb. 2006.

[9] M. Lustig, D. Donoho, and J.M. Pauly, "Sparse MRI: The application of compressed sensing for rapid MR imaging," *Magnetic Resonance in Medicine*, vol. 58, pp. 1182–1195, 2007.

[10] H. Jung, K. Sung, K.S. Nayak, E.Y. Kim, and J.C. Ye, "k-t FOCUSS: A general compressed sensing framework for high resolution dynamic MRI," *Magnetic Resonance in Medicine*, vol. 61, no. 1, pp. 103–116, 2009.

[11] S.G. Lingala, Yue Hu, E. DiBella, and M. Jacob, "Accelerated Dynamic MRI Exploiting Sparsity and Low-Rank Structure: k-t SLR," *Medical Imaging, IEEE Transactions on*, vol. 30, no. 5, pp. 1042–1054, May 2011.

[12] V. Singh and A.H. Tewfik, "Redundancy Encoding in Dynamic MR Imaging using Structured Sparsity," in *MICCAI Wshp. Sparsity Techniques in Medical Imaging*, 2012, pp. 1–8.

[13] N. Vaswani, "Kalman filtered Compressed Sensing," in *15th IEEE International Conference on Image Processing, 2008. ICIP 2008*, Oct. 2008, pp. 893–896.

[14] D. Angelosante, S.I. Roumeliotis, and G.B. Giannakis, "Lasso-Kalman smoother for tracking sparse signals," in *2009 Conference Record of the Forty-Third Asilomar Conference on Signals, Systems and Computers*, Nov. 2009, pp. 181–185.

[15] C. L. Webber and J. P. Zbilut, "Dynamical assessment of physiological systems and states using recurrence plot strategies," *Journal of Applied Physiology*, vol. 76, no. 2, pp. 965–973, 1994.

[16] S.G. Yuen, P.M. Novotny, and R.D. Howe, "Quasiperiodic predictive filtering for robot-assisted beating heart surgery," in *IEEE International Conference on Robotics and Automation, 2008. ICRA 2008*, May 2008, pp. 3875–3880.

[17] M.Salman Asif, Adam Charles, J. Romberg, and Christopher Rozell, "Estimation and dynamic updating of time-varying signals with sparse variations," in *2011 IEEE International Conference on Acoustics, Speech and Signal Processing (ICASSP)*, May 2011, pp. 3908–3911.

[18] Scott Shaobing Chen, David L. Donoho, and Michael A. Saunders, "Atomic decomposition by basis pursuit," *SIAM JOURNAL ON SCIENTIFIC COMPUTING*, vol. 20, pp. 33–61, 1998.

[19] S. Becker, J. Bobin, and E. J. Cands, "NESTA: a fast and accurate first-order method for sparse recovery," *SIAM Journal on Imaging Sciences*, vol. 4, no. 1, pp. 139, 2011.

[20] Z. Wang, A.C. Bovik, H.R. Sheikh, and E.P. Simoncelli, "Image quality assessment: from error visibility to structural similarity," *Image Processing, IEEE Transactions on*, vol. 13, no. 4, pp. 600 –612, april 2004.

[21] L. Ge, A. Kino, M. Griswold, C.A. Mistretta, J.C. Carr, and D. Li, "Myocardial perfusion MRI with sliding-window conjugate-gradient HYPR," *Magnetic Resonance in Medicine*, vol. 62, no. 4, pp. 835–839, 2009.